

DGS Loaded Substrate Integrated Waveguide Dual Mode Cavity Filter

Xiaohei Yan^{*}, Wenjing Mu, and Minjie Guo

Abstract—A novel substrate-integrated waveguide (SIW) dual-mode cavity bandpass filter with a loaded defected ground structure (DGS) is proposed. The SIW dual-mode cavity operates in two modes, TE_{110} and TE_{120} , and the field distribution of the TE_{110} mode is altered by installing a metal perturbation aperture in the middle of the cavity to bring its resonance frequency close to that of the TE_{120} mode, forming a bandpass filter with two resonance points in the passband. A DGS structure is embedded at the ground level of the SIW to introduce a transmission zero in the high-frequency rejection band, thus improving the rejection performance of the filter for the high-frequency rejection band. The simulated and measured results show that the center frequency of the filter is 3.75 GHz; the 3 dB bandwidth is 0.3 GHz; the relative bandwidth is 8%; the return loss is less than -15 dB; and the insertion loss in the passband obtained from the simulation is about -0.35 dB, while that obtained from the measurement is 0.4 dB lower than that of the simulation, and the filter has a transmission zero near the high-frequency stopband of 6 GHz, which enables the high-frequency parasitic passband to move away from the passband of the filter. Except for the passband, all other signals in the Sub-6 GHz band can be effectively suppressed by the filter. This design combines the SIW dual-mode cavity with the DGS structure to design the filter, which can realize the flexible adjustment of bandwidth and transmission zero point, and the design method is simple and innovative. The filter can be applied to the 5G n77 frequency band, which has a certain application value.

1. INTRODUCTION

In recent years, with the rapid development of communication technology and microwave devices, there has been a growing demand for efficient, compact, and high-performance filters. Filters play a crucial role in wireless communications, radar systems, and fiber optic communications for suppressing interfering signals, selecting specific frequency bands, and improving system performance. Therefore, the design and preparation of novel filter structures has become one of the hot topics in current research [1, 2].

Substrate Integrated Waveguide (SIW), as a new type of waveguide device, has attracted much attention due to its advantages of miniaturization, low loss, high reliability, and ease of integration, and these features have led to its wide application in the fields of filters and microwave integrated circuits [3–6]. Meanwhile, Defected Ground Structure (DGS), as a novel means of microwave device design, is widely used in frequency selectivity, spurious harmonic suppression, waveguide mode suppression, etc. [7–11].

In recent years, researchers have worked on the application of substrate-integrated waveguides and DGS structures to the design of microwave filters to realize higher-performance microwave filters [12–15]. Reference [12] proposes an in-line port-fed dual-mode substrate integrated waveguide filter, which utilizes metal tweak holes in the cavity to achieve the separation of the simple-parallel modes TE_{120} and TE_{210} to form a filter with two resonance points in the passband, and by changing the position

Received 24 August 2023, Accepted 27 October 2023, Scheduled 7 November 2023

* Corresponding author: Xiaohei Yan (yanxiaohei@gxnun.edu.cn).

The authors are with the School of Mathematics and Electronic Information Engineering, Guangxi Minzu Normal University, Chongzuo 532200, China.

of the metal tweak holes, the transmission zeros at different locations can also be achieved, but the relative bandwidth of the filter is small, and the parasitic passbands are close together. Reference [13] proposes a substrate-integrated waveguide filter with a dual-mode air resonant cavity, which utilizes an air resonant cavity and a bias-feeding method to achieve the excitation of the TM_{110} and TM_{210} to form a filter with two resonance points in the passband. The use of an air resonant cavity reduces the size of the filter, but the non-closed structure of the air resonant cavity also brings about a large insertion loss, and the filter's relative bandwidth is also smaller. Reference [14] proposes a substrate-integrated waveguide bandpass filter loaded with an E-type DGS structure, which utilizes the substrate-integrated waveguide as a transmission line, not as a resonant cavity. At this time, the substrate-integrated waveguide has the role of the high-pass, and the E-type DGS structure plays the role of the band-stop, which realizes that the parasitic passband is as far away as possible through the etching of multiple DGS structures on the ground of the substrate-integrated waveguide. The filter's relative bandwidth is larger, but the introduction of multiple DGS structures will inevitably bring about a greater insertion loss. Reference [15] proposes a compact substrate-integrated waveguide bandpass filter loaded with two open-ring DGS structures, which utilizes the direct coupling between the source and the load, the coupling of the open-ring DGS, and the TE_{110} mode of the waveguide to form multiple transmission paths between the source and the load. The filter has a good bandwidth, and the parasitic passbands are far away from each other.

In previous studies, more bandpass filters are obtained by perturbing multimode resonant cavities or loading multiple DGS structures into substrate-integrated waveguide transmission lines to form bandpass filters, while there are fewer studies on loading DGS structures into substrate-integrated waveguide multimode cavities to form bandpass filters with better stopband rejection. In this context, a DGS-loaded substrate-integrated waveguide dual-mode cavity filter is proposed in this paper. Experimental results show that the filter exhibits better performance in frequency selection and out-of-band rejection, providing a new idea and method for filter design in microwave and millimeter-wave fields.

2. FILTER STRUCTURE

This design adopts a single-layer substrate-integrated waveguide cavity structure, whose three-dimensional structure is shown in Figure 1, with a metal layer on the top and bottom sides and a

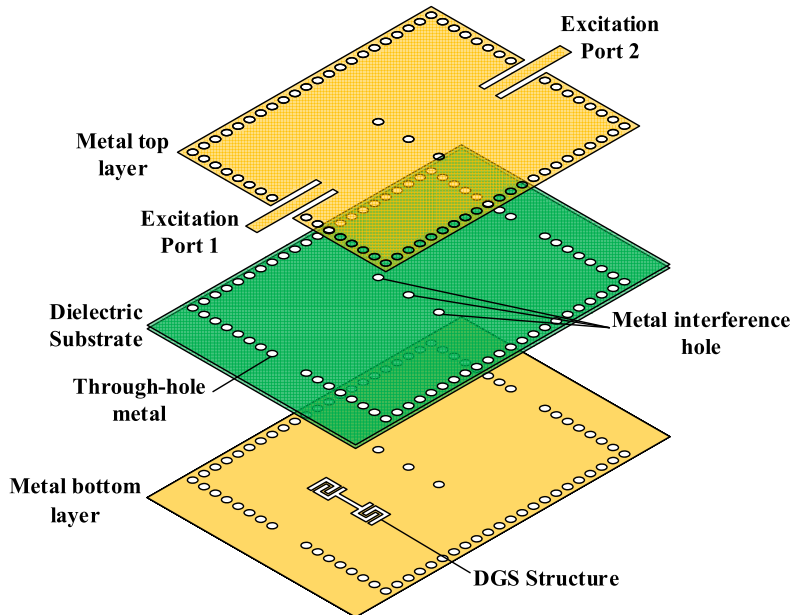


Figure 1. Decomposition of the filter structure.

dielectric layer in the middle (the material is Rogers 5880, which has a relative permittivity of 2.2 and a loss tangent of 0.0009). The substrate-integrated waveguide cavity is rectangular in shape as a whole and operates in both TE₁₁₀ and TE₁₂₀ modes, and the resonant frequency ratio between TE₁₂₀ and TE₁₁₀ can be adjusted by setting its aspect ratio. A metal perturbation hole is set in the middle of the cavity to change the field distribution of the TE₁₁₀ mode so that its resonant frequency is close to the TE₁₂₀ mode. A DGS structure is etched in the metal bottom layer (ground) of the substrate-integrated waveguide cavity, and the DGS structure adopts a nested U-shape structure. The DGS structure can introduce a transmission zero in the high-frequency rejection band of the filter, thus improving the rejection performance of the filter for the high-frequency rejection band. Of course, changes in the dimensions of the DGS structure will lead to changes in the location of the transmission zero point and changes in the high-frequency rejection performance of the high-frequency stopband. The shape of the metal layer of the filter is shown in Figure 2, and the final structural parameters after simulation optimization using simulation software HFSS are shown in Table 1.

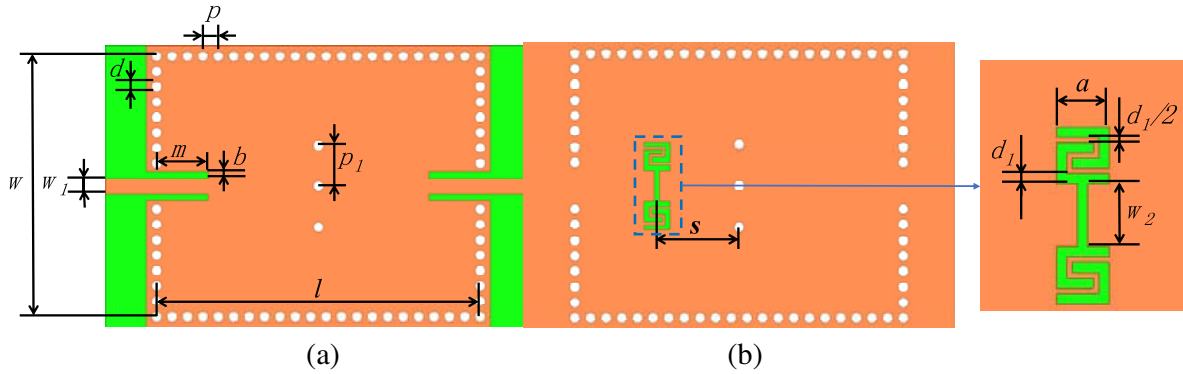


Figure 2. Dimensional drawings of the metal layers. (a) Metal top layer; (b) Metal bottom layer.

Table 1. Filter structural parameters (unit: mm).

$l = 63$	$w = 51$	$w_1 = 3$	$m = 10$
$b = 1.4$	$p = 3$	$d = 2$	$p_1 = 8$
$d_1 = 1$	$w_2 = 6$	$s = 15.75$	$a = 5$

3. FILTER DESIGN AND PRINCIPLE ANALYSIS

In this design, the substrate-integrated waveguide cavity operates in two modes, TE₁₁₀ and TE₁₂₀, and the resonant electric field distribution of the two modes is shown in Figure 3.

The resonant frequency f_{mn0} of the substrate-integrated waveguide cavity operating in the TE_{mn0} mode can be calculated from the relationship between the cavity dimensions and mode resonant frequency, which is:

$$f_{TE_{mn0}} = \frac{c_0}{2\sqrt{\epsilon_r}} \sqrt{\left(\frac{m}{w_{eff}}\right)^2 + \left(\frac{n}{l_{eff}}\right)^2} \quad (1)$$

where ϵ_r is the dielectric constant of the dielectric substrate; m and n are the number of modes along the width and length directions, respectively; w_{eff} and l_{eff} are the equivalent width and length of the SIW structure, which are defined as follows:

$$w_{eff} = w + \frac{d^2}{0.95p}, \quad l_{eff} = l + \frac{d^2}{0.95p} \quad (2)$$

where w is the center distance between two rows of circular holes on the wide side of the cavity, l the center distance between two columns of circular holes on the long side of the cavity, d the diameter of the

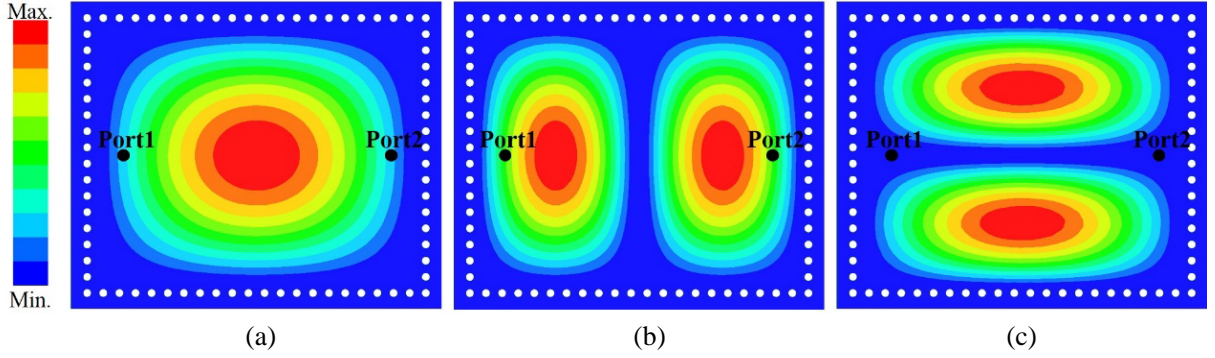


Figure 3. Electric field strength distribution in the cavity. (a) TE_{110} mode; (b) TE_{120} mode; (c) TE_{210} mode.

circular holes, and p the centroidal distance between adjacent circular holes. The resonance frequency ratio between TE_{120} and TE_{110} can be expressed as:

$$A = \frac{f_{120}}{f_{110}} = \frac{\sqrt{\left(\frac{1}{w_{eff}}\right)^2 + \left(\frac{2}{l_{eff}}\right)^2}}{\sqrt{\left(\frac{1}{w_{eff}}\right)^2 + \left(\frac{1}{l_{eff}}\right)^2}} = \sqrt{\frac{1 + 4\left(\frac{w_{eff}}{l_{eff}}\right)^2}{1 + \left(\frac{w_{eff}}{l_{eff}}\right)^2}} \quad (3)$$

In this design, the filter operates in the 5G n77 band, so the resonant frequency of TE_{120} is initially taken to be 3.8 GHz. The value of $\frac{w_{eff}}{l_{eff}}$ is 0.8, and the initial dimensions of the cavity can be calculated according to Eqs. (1), (2), and (3):

$$w \approx 51 \text{ mm}, \quad l \approx 63 \text{ mm} \quad (4)$$

Placing three metal perturbation holes in the middle position of the cavity length direction can change the electric field distribution of TE_{110} mode, so that its equivalent size decreases, and thus its resonance frequency migrates to the high-frequency direction. For the TE_{120} mode, its resonant frequency is not affected by the metal perturbation holes because its electric field at the middle position of the cavity length direction is almost zero. Figure 4 shows the electric field strength distribution in the substrate-integrated waveguide cavity containing metal scrambling holes. Obviously, the larger the spacing of the metal scrambling holes is, the larger the influence of the electric field is on the TE_{110} mode, which in turn causes its resonant frequency to migrate more in the high-frequency direction.

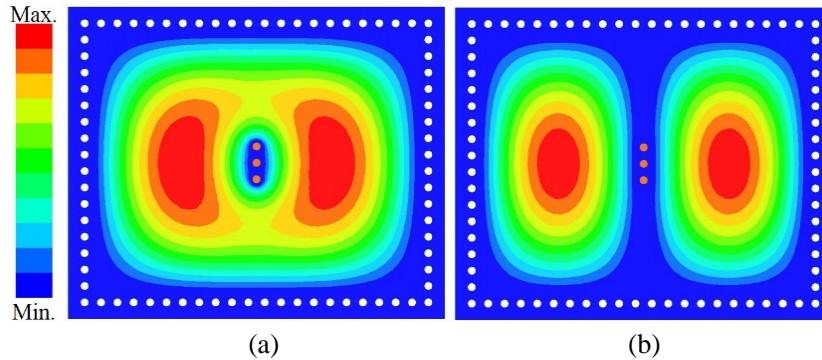


Figure 4. Electric field strength distribution in a cavity containing metallic perturbation holes. (a) TE_{110} mode; (b) TE_{120} mode.

In this design, the filter is fed by a $50\ \Omega$ microstrip line, and the transition form between the microstrip line and substrate-integrated waveguide cavity adopts a coplanar waveguide, so that the impedance matching between the two can be adjusted by the depth of the coplanar waveguide penetrating into the cavity, and the feed positions are located in the middle of the left and right sides in the direction of the width, i.e., Port 1 and Port 2 in Figure 3. For both TE_{110} and TE_{120} modes, the electric field at the excitation port is stronger and thus can be excited. For the TE_{210} mode, the electric field at the excitation port is almost zero and therefore cannot be excited. Of course, for higher-order resonant modes (e.g., TE_{220} , TE_{130} , TE_{310} , etc.) that can be excited, these higher-order resonant modes will form parasitic passbands in the high-frequency direction of the filter. If it is necessary to suppress these high-frequency parasitic passbands, they must be realized in a corresponding way.

DGS is a novel structure for microwave and millimeter-wave device design, which is essentially a defect pattern structure etched on the ground plane of microwave and millimeter-wave integrated circuits with band-resistive characteristics. By etching the DGS structure on the metal bottom surface of the substrate-integrated waveguide cavity, transmission zeros can be introduced to achieve high-frequency parasitic passband suppression.

The common structures of DGS are dumbbell type, spiral type, etc. The DGS structure used in this design is a nested U-type obtained by improving the dumbbell type, and its structure form is shown in Figure 5. The nested U-type structure increases the etching path compared to the dumbbell type, so it increases the equivalent capacitance and inductance and occupies a smaller area than the dumbbell type based on the same transmission zeros. At the same time, the nested U-type structure is easier to manufacture than the spiral type. The above two points are the main reasons for adopting the nested U-type structure in this design. According to the operating frequency and wavelength of the filter, the dimensions of the nested U-type DGS structure can be initially taken as:

$$d_1 = 1\ \text{mm}, \quad a = 5\ \text{mm}, \quad w_2 = 6\ \text{mm} \tag{5}$$

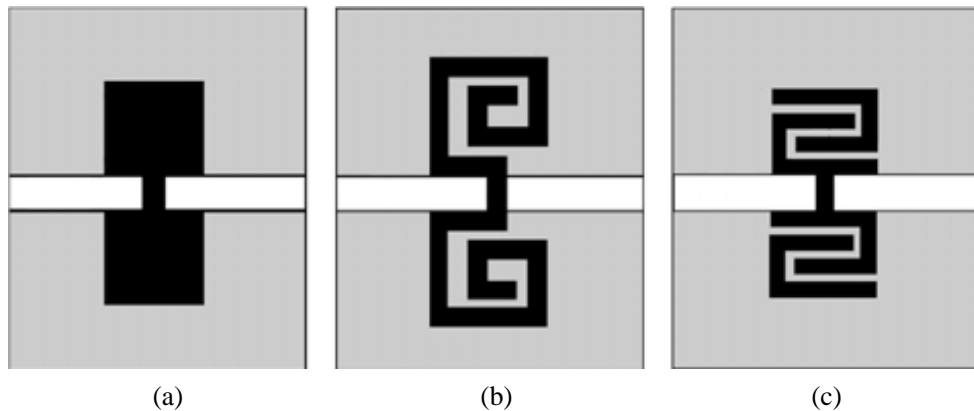


Figure 5. DGS structures. (a) Dumbbell; (b) Spiral; (c) Nested U-shaped.

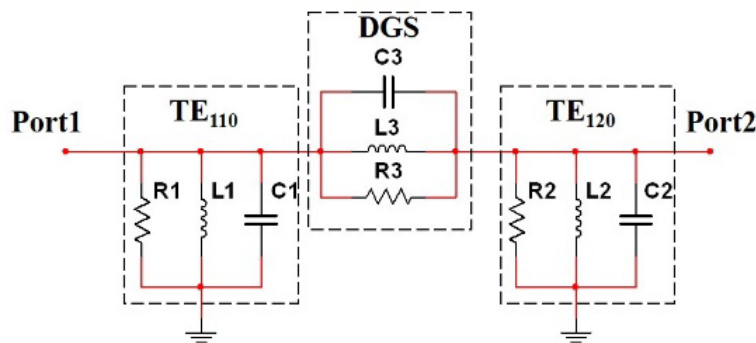


Figure 6. Equivalent circuit of the filter.

The equivalent circuit of the filter can be represented in Figure 6. The two resonant modes of the substrate-integrated waveguide cavity (TE_{110} and TE_{120}) can be equated to two LC parallel resonant circuits, which act as band-passes, and the DGS structure can be equated to an LC parallel resonant circuit connected in series between TE_{110} and TE_{120} , which acts as a band-stop. Thus, the filter can realize the effect of letting a signal of a specific frequency range pass and suppressing the signal of another specific frequency range.

4. RESULTS AND ANALYSIS

4.1. Simulation Results without DGS Loaded Filter

The simulated S -parameters of the filter (without DGS loaded) for different metal perturbation hole spacing (p_1) are given in Figure 7. It can be seen that there are two obvious resonance points in the passband, which correspond to the resonance frequencies of TE_{110} and TE_{120} modes, respectively. With the increase of p_1 from 6 mm to 9 mm, the bandwidth of the filter in the 5G n77 band becomes gradually smaller, and the passband slowly transitions from the double peaks, which are obviously recessed at 6 mm, to the flatter single peaks. The reason for this is that the increase in the spacing of the metallic perturbation holes increases the effect on the electric field distribution of the TE_{110} mode, which decreases its equivalent size, and thus the resonance frequency migrates toward the TE_{120} mode. For TE_{120} mode, its resonant frequency is not affected by the metal perturbation holes because its electric field is almost zero at the middle position of the cavity length direction. In Figure 7, the almost constant resonant frequency of TE_{120} mode and the migration of the resonant frequency of TE_{110} mode can be clearly observed. The filter forms a high-frequency parasitic passband above 6 GHz, and the presence of the parasitic passband can reduce the rejection performance of the filter in the high-frequency stopband. Similarly, this high-frequency parasitic passband also migrates toward higher frequencies as p_1 increases. This is because this parasitic passband is generated by the resonant frequency of the TE_{220} or TE_{130} mode, and the increase in the spacing of the metallic perturbation holes increases the effect on their electric field distribution. It should be noted that the increase of p_1 leads to the decrease of the filter bandwidth while the reflection coefficient in the passband decreases, and S_{11} is less than -25 dB when $p_1 = 8$ mm and less than -35 dB when $p_1 = 9$ mm. Considering both the bandwidth and reflection coefficient together, $p_1 = 8$ mm is taken in later experiments. The other parameters of the filter are shown in Table 1.

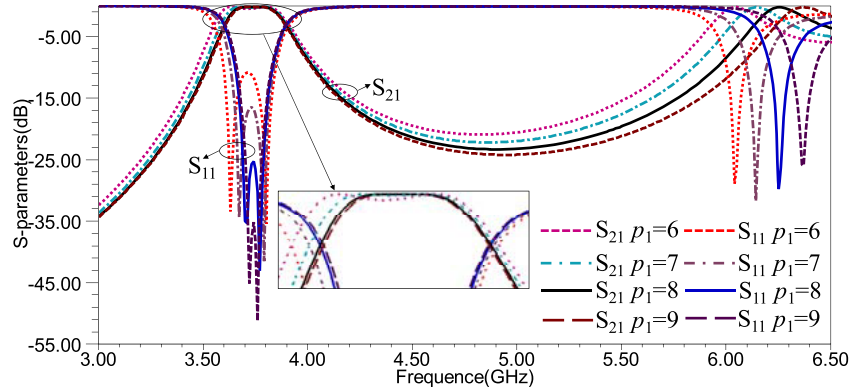


Figure 7. S -parameters of the filter obtained by simulation.

Figure 8 gives the electric field strength distribution of the without DGS loaded filter at different frequencies. It can be seen that at the passband center frequency of 3.75 GHz, the signal can pass through the filter smoothly, at which time the output signal is the result of the superposition by TE_{110} mode and TE_{120} mode; at the low-frequency rejection band of 2.4 GHz, the signal cannot pass through; at the high-frequency rejection band of 6 GHz, the signal can be stimulated in the filter to TE_{220} transmission mode, which has a stronger output signal at this time. This is consistent with the results reflected in the filter S -parameters.

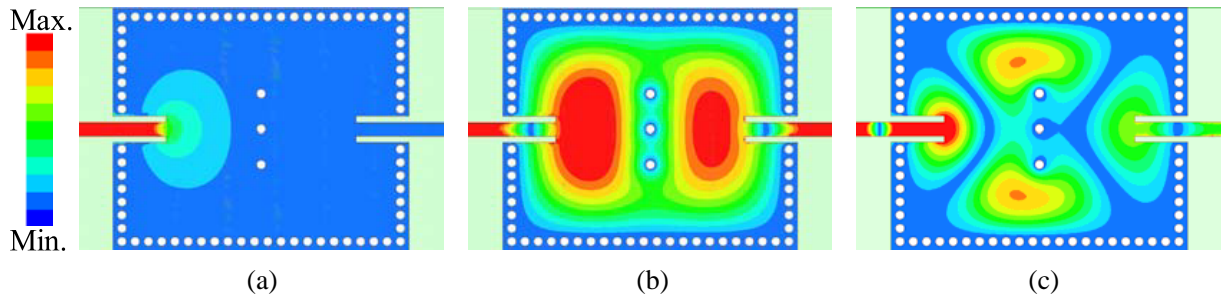


Figure 8. Electric field strength distributions of the without DGS loaded filter at different frequencies. (a) 2.4 GHz; (b) 3.75 GHz; (c) 6 GHz.

4.2. Simulation Results with DGS Loaded Filter

The DGS structure is a defect pattern etched on the metal bottom surface of the substrate-integrated waveguide dual-mode cavity, which has a band-reject characteristic, and by controlling its structural dimensions, it is possible to improve the rejection performance of the filter's rejection band by introducing a transmission zero at the corresponding frequency of the filter's rejection band. The DGS structure used in this design is a nested U-shape obtained by improving the dumbbell type. The nested U-shape structure increases the equivalent capacitance and inductance by adding the etch path compared to the dumbbell type and occupies a smaller area than the dumbbell type based on the same transmission zero point. The size of the DGS structure is related to the wavelength of the waveguide at the transmission zero point, which is initially taken to be half of the wavelength of the waveguide at the transmission zero point. This design expects to produce a transmission zero near 6 GHz with a waveguide wavelength of about 34mm and a half waveguide wavelength of about 17mm, so the preliminary dimensions of the DGS structure are taken as the result shown in Equation (5).

The simulated S -parameters of the filter with different w_2 parameter values are given in Figure 9. It can be seen that loading the DGS structure introduces a transmission zero near 6 GHz, which effectively improves the rejection performance of the filter in the high-frequency stopband (4 ~ 6 GHz). However, the reflection coefficient in the passband of the filter deteriorates from -25 dB to -15 dB, due to a certain degree of energy leakage caused by the introduction of the DGS structure. The value of w_2 is varied from 5 mm to 7 mm; the transmission zero (denoted as f_{zero}) migrates to the low-frequency direction; $f_{zero} = 6.03$ GHz for $w_2 = 6$ mm, and $f_{zero} = 5.94$ GHz for $w_2 = 7$ mm. This is because an increase in w_2 leads to an increase in the equivalent capacitance and inductance of the DGS structure. As the value of w_2 is varied from 5 to 7 mm, the filter's S_{21} in the range of 5 to 6 GHz gets smaller, and the signal rejection performance in this range becomes better, but the filter's S_{21} in the range of 4

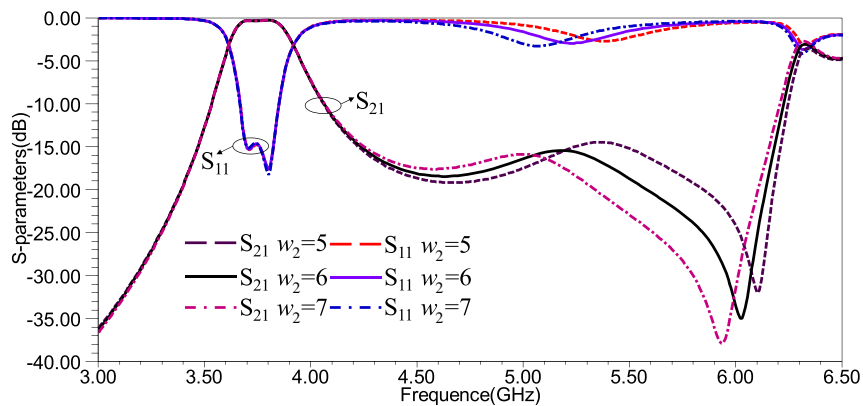


Figure 9. Effect of w_2 parameter on the S -parameters of the filter.

to 5 GHz gets larger, and the signal rejection performance in this range becomes worse. Combining the above factors and design expectations, the final $w_2 = 6$ mm.

The simulated S -parameters of the filter for different d_1 parameter values are given in Figure 10. It can be seen that the transmission zero (f_{zero}) migrates to the low-frequency direction when the d_1 parameter value is varied from 0.9 mm to 1.1 mm, because the increase of d_1 leads to the increase of the equivalent capacitance and inductance of the DGS structure. d_1 parameter value is varied from 0.9 mm to 1.1 mm; S_{21} of the filter in the range of 5–6 GHz becomes smaller; and the rejection performance of the signals in this range becomes better, but the filter S_{21} in the range of 4–5 GHz becomes larger, and the rejection performance of the signal in this range becomes worse. Meanwhile, the reflection coefficient in the passband of the filter deteriorates from -16 dB to -12 dB when d_1 is changed from 0.9 mm to 1.1 mm, because the larger the d_1 size is, the more energy leakage is generated from the DGS structure. By combining the above factors and design expectation, the final $d_1 = 1$ mm is taken as the final size.

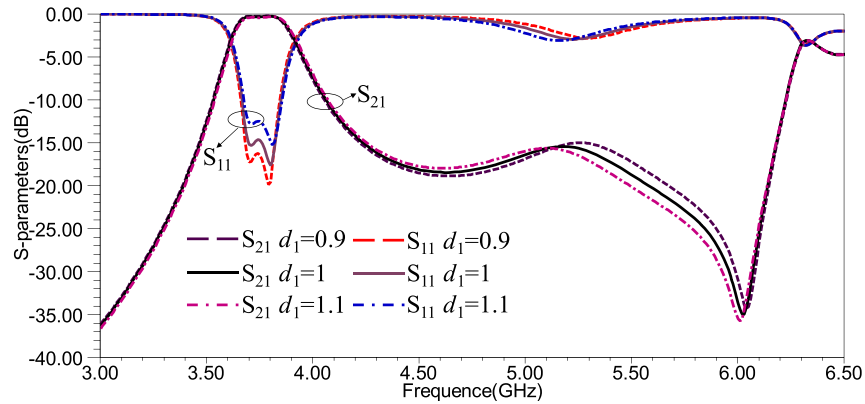


Figure 10. Effect of d_1 parameter on the S -parameters of the filter.

The electric field strength distributions of the filter with DGS loading at different frequencies are given in Figure 11. It can be seen that at the passband center frequency of 3.75 GHz, the signal is almost unaffected by the DGS structure and can pass through the filter smoothly; at the low-frequency blocking band of 2.4 GHz, the signal cannot pass through; and at the high-frequency blocking band of 6 GHz, the signal can be suppressed efficiently by the DGS structure, and at this time, the signal cannot pass through. The above results are consistent with those reflected in the S -parameters of the filter.

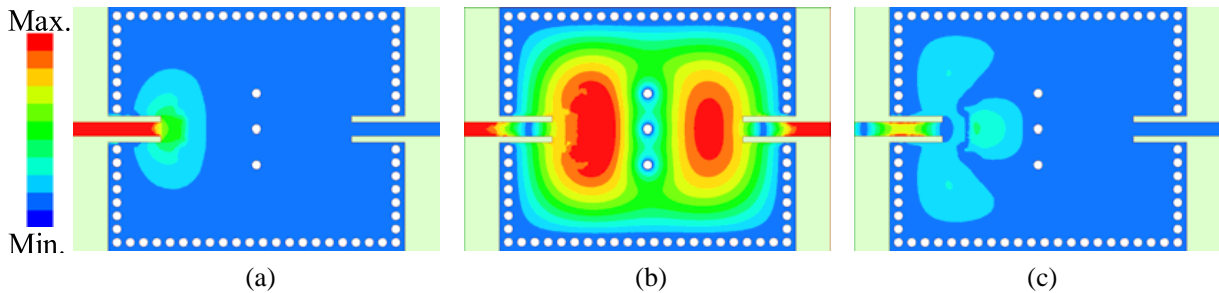


Figure 11. Electric field strength distribution at different frequencies with DGS-loaded filters. (a) 2.4 GHz; (b) 3.75 GHz; (c) 6 GHz.

4.3. Comparison of Simulation and Test Results

According to the dimensions listed in Table 1, the physical filter was processed using the printed circuit board (PCB) process, and the physical filter is shown in Figure 12. During physical testing, it is necessary to solder SMA-KHD coaxial connectors onto the input and output ports of the filter and

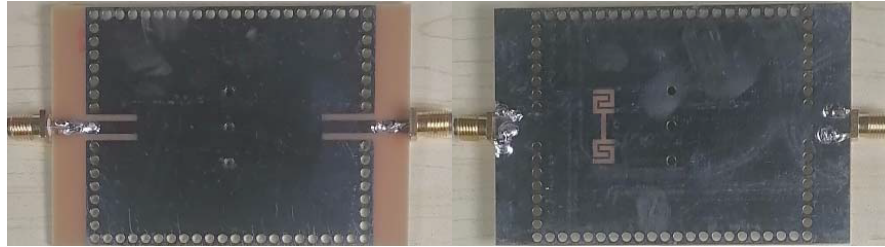


Figure 12. Filter object.

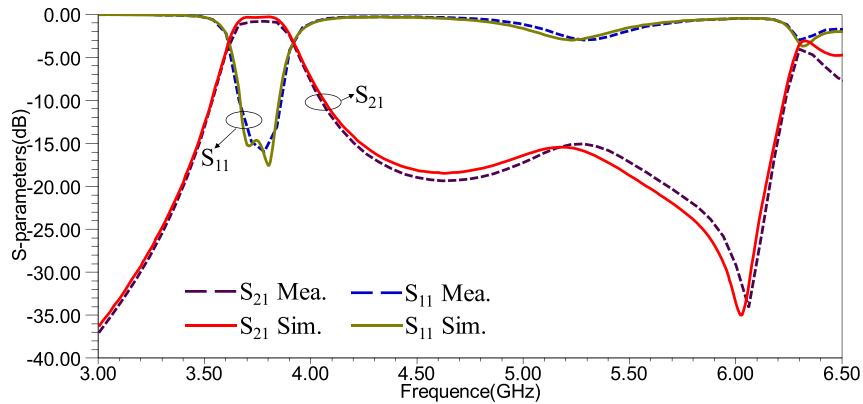


Figure 13. Simulated and measured filter S -parameters.

connect them to an Agilent E8363C network vector analyzer for measurement. The simulated and measured S -parameter results of the filter are shown in Figure 13. It can be seen that the overall trends of the measured and simulated S -parameter curves are consistent; the center frequency of the filter is 3.75 GHz; the 3 dB bandwidth is 0.3 GHz; the relative bandwidth is 8%; and the return loss is less than -15 dB. The insertion loss in the passband obtained in the simulation is about -0.35 dB, and that obtained in the actual measurement is 0.4 dB lower than the simulated value. The measured transmission zero position is slightly higher than the simulated value. The difference between the measured and simulated values is mainly attributed to the processing error, dielectric loss, and conversion structure loss.

A comparison of the performance of the proposed filter with similar filters in the references is given in Table 2. From the table, it can be obtained that the proposed filter has better relative bandwidth, lower insertion loss, better out-of-band rejection performance, and also the parasitic passband is far away.

Table 2. Comparison with similar filters in the literature.

Refs.	F_0 (GHz)	Insertion Loss (dB)	FBW (%)	Parasitic passband distance
[12]	15	0.92	3.8	near
[13]	3.38	3.02	1.5	far
[14]	26.6	2	21.3	near
[15]	4.9	1.1	9.2	far
This work	3.75	0.75	8	far

5. CONCLUSION

In this paper, a novel substrate-integrated waveguide (SIW) dual-mode cavity filter with a loaded defected ground structure (DGS) is proposed. The SIW dual-mode cavity operates in two modes, TE_{110} and TE_{120} , and the field distribution of the TE_{110} mode is altered by installing metal perturbation holes in the middle of the cavity to make its resonance frequency close to that of the TE_{120} mode, to form the band-pass filter with two resonance points in the passband. At the same time, the filter bandwidth can be adjusted by adjusting the spacing of the metal scrambling holes. The DGS structure is embedded at the ground surface of the SIW to introduce a transmission zero near the high-frequency stopband at 6 GHz, thus improving the rejection performance of the filter for the high-frequency stopband. Similarly, the adjustment of the position of the transmission zero can be realized through the adjustment of the size of the DGS structure, and then the adjustment of the rejection performance of the stopband can be realized. The simulated and measured results show that the center frequency of the filter is 3.75 GHz; the 3 dB bandwidth is 0.3 GHz; the relative bandwidth is 8%; the return loss is less than -15 dB; the insertion loss in the passband obtained by the simulation is better than -0.35 dB; and the insertion loss obtained by the measurement is lower than the simulation value by 0.4 dB. This design combines the SIW dual-mode cavity with the DGS structure to design the filter, which can realize the flexible adjustability of the bandwidth and transmission zero of the filter, and the design method is simple and innovative. The filter can be used in the 5G n77 frequency band, which has a certain application value.

ACKNOWLEDGMENT

This work is supported by the Basic Research Ability Improvement Project for Young and Middle-aged Teachers in Guangxi Universities (No. 2023KY0793 and No. 2023KY0796) and the Guangxi Natural Science Foundation (No. 2022JJB150010).

REFERENCES

1. Bozzi, M., A. Georgiadis, and K. Wu, "Review of substrate-integrated waveguide circuits and antennas," *IET Microwaves, Antennas & Propagation*, Vol. 5, No. 8, 909–920, 2011.
2. Chen, X.-P. and K. Wu, "Substrate integrated waveguide filter: Basic design rules and fundamental structure features," *IEEE Microwaves Magazine*, Vol. 15, No. 5, 108–116, 2014.
3. Saghati, A. P., A. P. Saghati, and K. Entesari, "Ultra-miniature SIW cavity resonators and filters," *IEEE Transactions on Microwave Theory and Techniques*, Vol. 63, No. 12, 4329–4340, 2015.
4. Schorer, J., J. Bornemann, and U. Rosenberg, "Mode-matching design of substrate mounted waveguide (SMW) components," *IEEE Transactions on Microwave Theory and Techniques*, Vol. 64, No. 8, 2401–2408, 2016.
5. Xu, S., K. Ma, F. Meng, and K. S. Yeo, "Novel defected ground structure and two-side loading scheme for miniaturized dual-band SIW bandpass filter designs," *IEEE Microwave and Wireless Components Letters*, Vol. 25, No. 4, 217–219, 2015.
6. Khandelwal, M. K., B. K. Kanaujia, and S. Kumar, "Defected ground structure: Fundamentals, analysis, and applications in modern wireless trends," *Int. J. Antennas Propag.*, Vol. 2017, 2018527, 2017.
7. Kumar, C. and D. Guha, "Reduction in cross-polarized radiation of microstrip patches using geometry-independent resonant-type defected ground structure (DGS)," *IEEE Trans. Antennas Propag.*, Vol. 63, No. 6, 2767–2772, 2015.
8. Kumar, C. and D. Guha, "Asymmetric geometry of defected ground structure for rectangular microstrip: A new approach to reduce its cross-polarized fields," *IEEE Trans. Antennas Propag.*, Vol. 64, No. 6, 2503–2506, 2016.
9. Wei, K., J. Y. Li, L. Wang, R. Xu, and Z. J. Xing, "A new technique to design circularly polarized microstrip antenna by fractal defected ground structure," *IEEE Trans. Antennas Propag.*, Vol. 65, No. 7, 3721–3725, 2017.

10. Wei, K., J. Y. Li, L. Wang, Z. J. Xing, and R. Xu, "Mutual coupling reduction by novel fractal defected ground structure bandgap filter," *IEEE Trans. Antennas Propag.*, Vol. 64, No. 10, 4328–4335, 2016.
11. Sahu, S. K., S. Sahu, and G. Palai, "Experimentally validated of defected microstrip structure to realize band stop filter based on capacitively loaded loop resonators," *Optik*, Vol. 158, 610–616, 2018.
12. Chu, P., W. Hong, M. Tuo, et al., "In-line ports dual mode substrate integrated waveguide filter with flexible responses," *IEEE Microwave and Wireless Components Letters*, Vol. 28, No. 10, 882–884, 2018.
13. Tomassoni, C., L. Silvestri, A. Ghiotto, et al., "Substrate-integrated waveguide filters based on dual-mode air-filled resonant cavities," *IEEE Transactions on Microwave Theory and Techniques*, Vol. 66, No. 2, 726–736, 2018.
14. Li, J., W. Zheng, X. Wei, et al., "Millimeter-wave substrate integrated waveguide bandpass filters based on stepped-impedance E-shaped defected ground structures," *International Journal of RF and Microwave Computer-Aided Engineering*, Vol. 32, No. 11, 126–138, 2022.
15. Shen, W., W. Y. Yin, and X. W. Sun, "Compact substrate integrated waveguide (SIW) filter with defected ground structure," *IEEE Microwave and Wireless Components Letters*, Vol. 21, 83–85, 2011.